Journal of Low Temperature Physics
https://doi.org/10.1007/s10909-022-02918-2

A Superconducting RF Low-Pass Filter Based on Ti/TiN Artificial Transmission Line for Detector and Qubit Readout

Y. Chen[1] · X. Dai[1] · J. Hu[1] · Q. He[2] · H. Gao[2] · X. Yang[1] · Y. Wang[1] · L. F. Wei[2] · M. R. Vissers[3] · J. Gao[3]

Received: 31 October 2021 / Accepted: 1 November 2022

Abstract

Cryogenic detector and qubit readout systems often include radio-frequency low-pass filters (LPFs) at the input/output paths to protect the sensitive devices from stray radiation traveling down the coaxial lines. For this application, a popular solution is to use custom-made copper powder filters, which are LPFs with injection of copper powder-loaded epoxy. They are very effective in attenuating high frequency (THz and far infrared) radiation but often introduce a few dBs of undesired insertion loss at the readout band below 10 GHz. Here, we describe a LPF design concept based on low-T_c ($\approx$ 700 mK) Ti/TiN superconducting artificial (lumped-element-loaded) transmission lines. We carefully design the unit inductance L_u and unit capacitance C_u to make the cut-off frequency $f_c = 1/(\pi\sqrt{L_u C_u}) \approx 30$ GHz and the characteristic impedance $Z_0 = \sqrt{L_u/C_u} \approx 50$ Ohm. Above the gap frequency ($\approx$ 50 GHz), the transmission line behaves as a lossy line made of normal metal which naturally attenuates the high-frequency radiations. In addition, the cavity resonances and spurious pass-bands at high frequencies can be effectively suppressed by adding a layer of microwave absorber below the substrate and by introducing an aperiodic loading of unit structures. A detailed design and electromagnetic simulation using realistic material parameters are presented. Our LPF design offers the advantages of close-to-zero insertion loss below 10 GHz, precise and sharp frequency roll-off, and linear phase response. The LPF can be placed in a separate package with compact size and easily connected to other superconducting circuits.

Keywords Low-pass filter · Artificial transmission line · Lumped transmission line

✉ Y. Wang
qubit@swjtu.edu.cn

[1] Quantum Optoelectronics Laboratory, School of Physics Science and Technology, Southwest Jiaotong University, Chengdu 610031, China

[2] Information Quantum Technology Laboratory, School of Information Science and Technology, Southwest Jiaotong University, Chengdu 610031, China

[3] National Institute of Standards and Technology, Boulder, CO 80305, USA

Published online: 29 November 2022

1 Introduction

Radio-frequency (RF) low-pass filters (LPFs) are an indispensable part of cryogenic microwave circuit systems. For example, LPFs are used in superconducting quantum computing to attenuate stray infrared photons and preserve the qubit coherence [1–5]. For this application, a popular solution is to use custom-made metal powder filters [6–8], with the central conductor placed in metal powder and epoxy filling. Fine powder particles (e.g., copper powder, aluminum powder, stainless steel powder) have a huge effective surface area, and the RF signal is attenuated by the skin effect. The filter characteristics depend on the composition of the filler and the size of the device [9]. To reduce the cut-off frequency, one can cascade the metal powder filters with external lumped-element LPFs [10–12]. The metal powder filters are very effective in attenuating high frequency (THz and far infrared) radiations but are difficult to design with repeatable performance and often introduce a few dBs of undesired insertion loss at the pass-band below 10 GHz. Furthermore, they are bulky and not integratable with qubit/detector devices. Therefore, a high-performance RF LPF with compact size is preferred for scaling up superconducting devices.

In this paper, we propose a design of superconducting RF low-pass filter based on an artificial transmission line (loaded with reactive elements, also known as lumped-element transmission line) made in coplanar waveguide (CPW) technology. It consists of a low-T_c (700 mK) Ti/TiN feed-line with high kinetic inductance and periodic units of interdigitated capacitor (IDC) fingers placed on both sides of the central strip. The artificial transmission line has a cut-off frequency which is determined by the design parameters of the unit cell. The transmission line is expected to become lossy above the gap frequency set by the T_c of the Ti/TiN film. We also use a microwave absorber (ECCOSORB-MF110) and aperiodic unit structures to suppress the cavity resonances and the spurious pass-bands. We simulate and study the transmission characteristics of the designed LPF (placed in a rectangular metallic enclosure) in a wide frequency range. The results show that our LPF device has a cut-off frequency near 30 GHz with insertion loss lower than 0.2 dB below 10 GHz and more than 30 dB attenuation above the cut-off frequency up to at least 200 GHz.

2 Principle

Figure 1 shows a lossless artificial transmission line with periodic structures of unit capacitance C_u and unit inductance L_u. From the telegraph equation [13], one can derive that the characteristic impedance and cut-off frequency of the artificial transmission line, which are given by:

$$Z_0 = \sqrt{\frac{L_u}{C_u}} \qquad f_c = \frac{1}{\pi\sqrt{L_u C_u}} \tag{1}$$

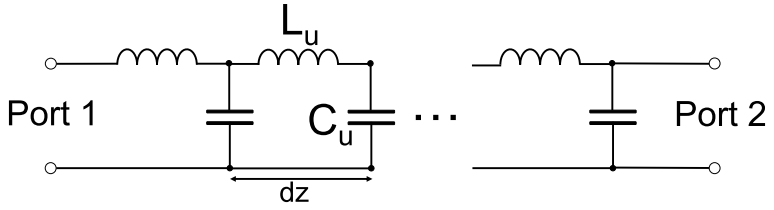

Fig. 1 A two-port lossless lumped transmission line with periodic loadings of unit inductance L_u and unit capacitance C_u

This cut-off frequency f_c, also known as Bragg frequency, is a function of how electrically small the unit cell is. Well below f_c, where the wavelength is much longer than the lumped unit length, the artificial transmission line becomes an approximation to a continuous transmission line. Above f_c, there are no traveling wave solutions and the lumped transmission line behaves as a LPF, which is the basis for our LPF design in this paper. Previously, the superconducting artificial transmission line is mainly used in broadband parametric amplifier and tunable coupler designs [14–16], because it has several advantages including low dissipation, compact size, tunable characteristic impedance and natural suppression of higher-order pump harmonics.

3 Design and Simulation

In our design, the target cut-off frequency is 30 GHz, and the characteristic impedance is 50 Ohm. This sets the unit inductance $L_u = 0.53$ nH and unit capacitance $C_u = 0.21$ pF according to Eq. 1. As shown in the appendix, we can take a separate 1-port simulation to obtain C_u and L_u. To reduce the device size, the feed-line is designed to be made from a thin ($\approx$ 80 nm-thick) superconducting Ti/TiN film [18] with sheet kinetic inductance $L_k = 15$ pH/sq and the designed feed-line width is 10 μm. This approximately sets the unit length to 220 μm since the inductance is dominated by the feed-line despite the IDC part also contributing with some inductance. The IDC is made from thick superconducting films of aluminum (Al), which are modeled as lossless metal with little kinetic inductance $\approx$ 0.2 pH/sq. The IDC can have various designs to have the same unit capacitance to the ground. In Fig. 2, we show three typical designs of the unit: wide finger, narrow finger and leaf-shaped finger [14], which have approximately the same unit capacitance. The wide finger is wider and shorter, the narrow finger is narrower and longer, and the leaf-shaped finger has small fingers growing on the main finger.

We use Sonnet EM Software [19] to simulate the transmission (S_{21}) of an 8-unit artificial transmission line in the superconducting state. The main part of the filter is designed to be placed in a rectangular metallic enclosure (2 mm $\times$ 3 mm), so we use perfect electric conductor (PEC) boundary conditions for all simulation box walls. Assembled with RF connectors (not included in the simulation), one can make a separate and compact package which can be easily inserted into the microwave

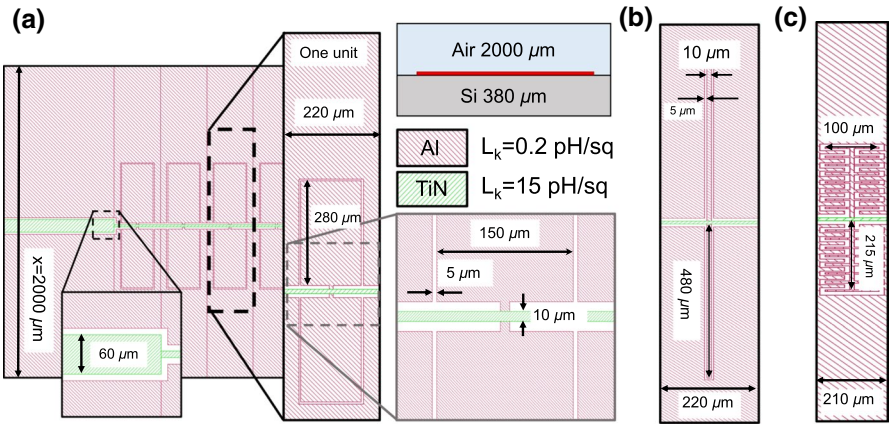

Fig. 2 (color online) The detailed design of three different units: **a** Wide finger, **b** Narrow finger, and **c** Leaf-shaped finger. Each unit has approximately the same inductance and capacitance. The green line represents the feed-line with $L_k = 15$ pH/sq, and the red area represents aluminum with $L_k = 0.2$ pH/sq. The metal film is placed on top of 380 μm thick Si substrate ($\epsilon_r = 11.44$) [17] and below an air gap (2 mm thick)

circuits at low temperature. The results for the above three typical unit designs are plotted in Fig. 3a, which generally show similar transmission characteristics and severe transmission leakage at high frequencies. As designed, the three S_{21} curves have approximately the same cut-off frequency at about 30 GHz and the insertion loss is close to zero below 15 GHz. Between about 30 GHz and 70 GHz, we can observe a few sharp resonance peaks, which can be attributed to cavity resonances because the metal film and Si substrate effectively form a rectangular cavity. We

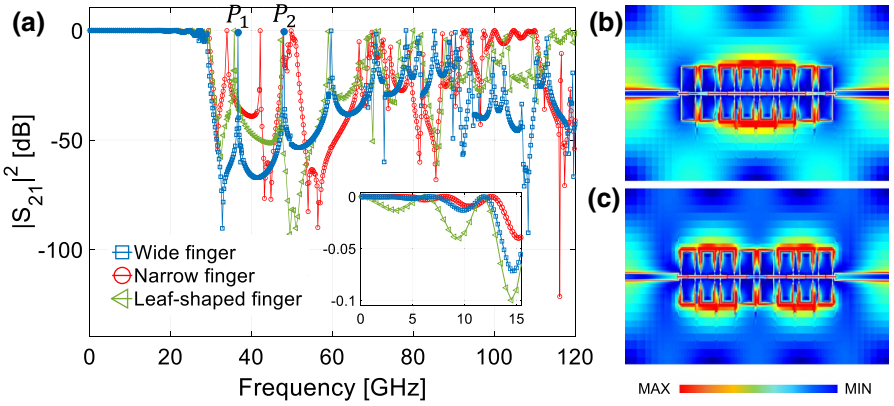

Fig. 3 (color online) **a** The simulated transmissions of 8-unit artificial transmission lines for 3 different unit designs: wide finger (blue curve), narrow finger (red curve) and leaf-shaped finger (green curve). All curves show similar features with cavity resonances and spurious pass-bands. **b** The simulated current density distribution at P_1 (36.66 GHz) for 8-unit wide finger design. **c** The simulated current density distribution at P_2 (47.97 GHz)

simulate the current density distribution at the first two obvious resonances, P_1 (36.66 GHz) and P_2 (47.97 GHz), on the blue curve (wide finger design). As shown in Fig. 3b and c, both of the current distributions show standing wave patterns, indicating that P_1 and P_2 correspond to the resonance frequencies of TE_{102} and TE_{103} modes. Actually, several cavity resonances can occur and the resonance frequencies are given by:

$$f_{mnp} = \frac{c}{2\sqrt{\varepsilon_r \mu_r}} \sqrt{\left(\frac{m}{x}\right)^2 + \left(\frac{n}{y}\right)^2 + \left(\frac{p}{z}\right)^2}, \tag{2}$$

where x, y, z are the dimensions of the cavity, and the indices m, n, p refer to the number of variations in the standing wave pattern along x-, y-, z-direction, respectively. The predicted resonances at $f_{102} = 36.95$ GHz and $f_{103} = 49.58$ GHz agree well with the simulated values. Note that the predicted first resonance $f_{101} = 26.65$ GHz is also observed in the pass-band (see the inset of Fig. 4a). Besides, one can also see a rising profile (above around 50 GHz) to a spurious pass-band (with multiple resonances) between about 70 GHz and 110 GHz. This is mainly due to the fact that the periodic unit is not composed of pure capacitance and inductance. The designed unit is actually a distributed element, which will cause undesired harmonics at higher frequencies. We take the wide finger design for further investigation because it has a simple structure and generally has lower transmission background.

4 Improvement

In this section, we analyze a few approaches to improve the performance of designed LPF. First, we use microwave-absorbing material to damp cavity resonances and radiation [20]. At cavity resonance frequencies, the cavity can provide a secondary

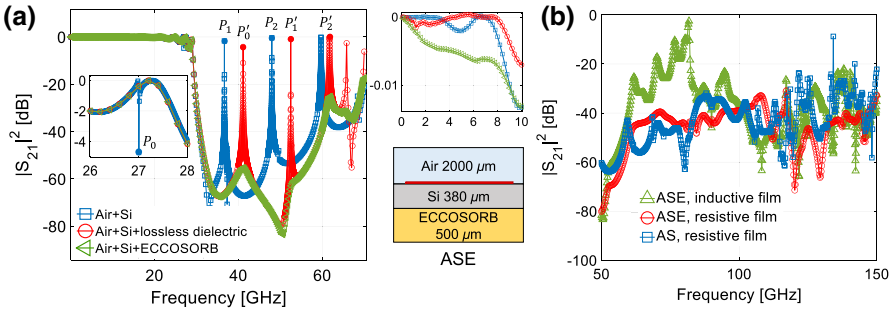

Fig. 4 (color online) **a** Simulated transmission with and without ECCOSORB below Si substrate. The parameters of ECCOSORB-MF110 at 10 GHz are: relative permittivity (permeability) 2.9 (1.0) and dielectric (magnetic) loss tangent 0.04 (0.1). The absorber parameters are actually frequency-dependent but are set constant in our simulation for simplicity. With the absorber, the cavity resonances are suppressed while not affecting the primary pass-band. **b** Comparison of the simulated transmission of LPF with resistive film (above gap frequency) and lossless film. A, S and E represent air layer, silicon substrate and ECCOSORB, respectively

coupling path between the input and output ports. The simulation shows the field distribution is significantly enhanced inside and at the cavity boundaries; therefore, the resonating energy can be effectively removed if we treat the back of silicon wafer with a microwave absorber. Figure 4a shows the transmission (green curve) when we place a thin layer of high loss ECCOSORB-MF110 [21] under the Si substrate. The magnitude of the cavity resonance peak is greatly reduced, comparing to the case without absorber (blue curve). In addition, the cavity resonances are shifted to higher values since the effective dielectric constant of the substrate cavity is lowered. For example, P_0 (27.00 GHz), P_1 (36.66 GHz) and P_2 (47.97 GHz) move up to $P_0^{'}$ (41.12 GHz), $P_1^{'}$ (52.48 GHz) and $P_2^{'}$ (61.73 GHz), respectively. This can be seen more clearly from the red curve in Fig. 4a, which plots the transmission for the case of adding a layer of lossless dielectric (with the same parameters with ECCOSORB-MF110 but no loss) under Si substrate. The red and green curves show remarkable difference only in the magnitude of the resonances. The above results show that the lossy absorber can effectively attenuate the cavity resonances while nearly not affecting the primary pass-band and the cut-off frequency. This is because the electromagnetic field of the primary signal is mainly guided by the CPW transmission line and mostly distributed inside the lossless Si substrate. Compared to cavity resonances due to perfect electric conducting box, the pass-band signal is less affected by the ECCOSORB. However, some practical issues need to be considered if the LPF using ECCOSORB is not placed in a separate package but integrated on the same chip with detectors/qubits. The simulation using typical design parameters shows that the internal quality factor Q_i will drop to about 40×10^3 for a 2 GHz resonator placed on top of Si substrate with lossy layer underneath. The high-frequency signals attenuated by the lossy layer may also cause heat and introduce extra thermal noise. Therefore, for on-chip applications, the lossy layer should be removed or at least placed a distance away from qubit/resonator.

Second, we take advantage of the properties of low T_c superconducting material. In our design, the feed-line is made of a thin superconducting Ti/TiN film with $T_c \approx 700$ mK and kinetic inductance $L_k = 15$ pH/sq, the IDC is made of a thick superconducting Al film with $T_c \approx 1.2$ K and kinetic inductance $L_k = 0.2$ pH/sq. There are all experimentally measured values. According to the BCS theory, the superconducting energy gap $2\Delta \approx 3.5 K_B T_c$ gives gap frequency of 50 GHz for TiN and 90 GHz for Al. An input photon of energy above gap frequency can directly break Cooper pairs, indicating the feed-line and IDC will become absorptive above 50 GHz and 90 GHz, respectively. For simplicity, the sheet resistance of the feed-line is set at $R_s = L_k \pi \Delta / \hbar = 7.5$ Ohm/sq [22] above 50 GHz and the Al film is set at 0.17 Ohm/sq above 90 GHz. In Fig. 4b, we compare the simulation results for three different situations: resistive feed-line (red curve), inductive feed-line (green curve) and resistive feed-line but removing the lossy layer (blue curve). We can see the transmission is generally the lowest and the fluctuation is suppressed in the stop-band for a resistive feed-line with ECCOSORB, although the superconducting gap of TiN directly provides a lot attenuation in the stop-band.

Third, we use aperiodic structures to suppress spurious pass-bands [23–25]. The IDC finger shows transmission zeros at frequencies corresponding to its length being

an integer multiple of quarter-wavelength. If we change the length of the IDC finger in steps, a series of transmission zeros at different frequencies will be generated, which can help suppress the spurious pass-bands. As shown in Fig. 5a, the aperiodic structure design contains eight units of wide IDC fingers with gradually changing lengths from 360 μm to 150 μm in steps of 30 μm. The simulated transmission is shown in the red curve in Fig. 5b. Compared to the periodic structure (blue curve), the aperiodic structure has a lower transmission in the stop-band at a cost of slower roll-off. The cut-off frequency is also lowered to about 25 GHz because f_c is limited by the largest loading unit. For both designs, the transmission is generally below −30 dB in the stop-band up to at least 200 GHz and the insertion loss is less than 0.2 dB in the pass-band below 10 GHz. Based on this aperiodic structure design, we also increase the number of units from 8 to 16 and place the LPF in a larger box (2 × 5 mm). This brings more attenuation in stop-band, which can be seen in the green curve in Fig. 5b. Between 50 and 200 GHz, the 16-unit design has a 4 dB lower transmission than the 8-unit design on average. This is reasonable since the total length of the feed-line (including the absorber) is increased. However, the transmission in the stop-band has rising profile with increasing frequency for all designs,

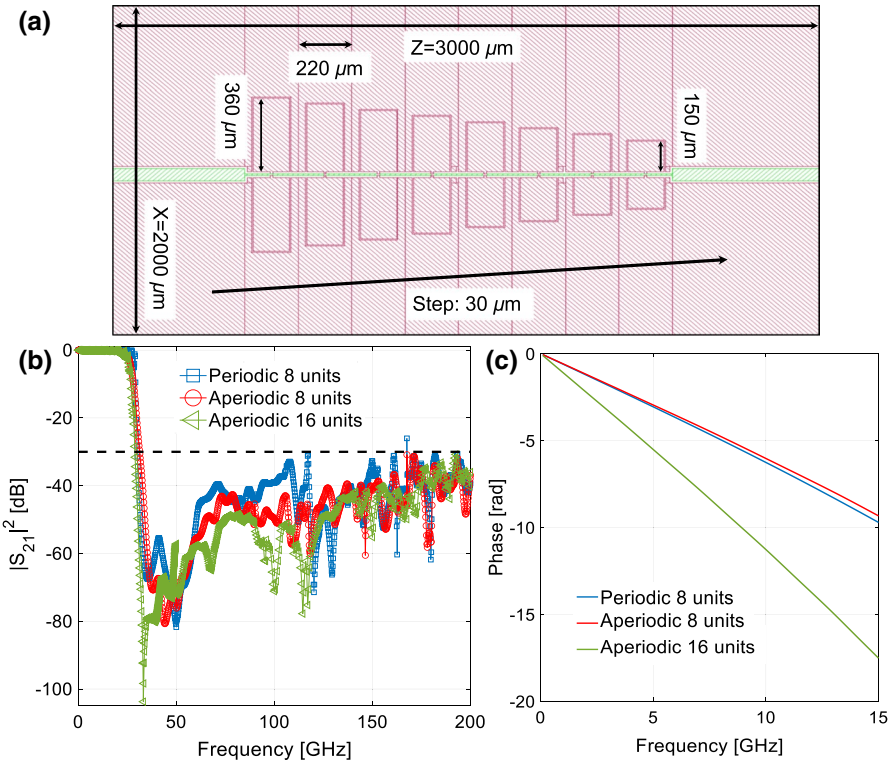

Fig. 5 (color online) **a** 8-unit design of aperiodic structure with an average unit impedance 50 Ohm. **b** Simulated transmissions for periodic 8-unit design, aperiodic 8-unit design, and aperiodic 16-unit design. **c** The designed filters show approximately linear phase response in the pass-band

indicating it is really challenging to attenuate radiation at even higher frequency above 200 GHz. Note that the insertion loss is still less than 0.2 dB in the pass-band below 10 GHz. Figure 5c plots the phase response for these LPF designs in the pass-band up to 15 GHz. The linear phase shift with frequency shows that our LPF is suitable to be used in phase-sensitive readout.

5 Conclusion

In conclusion, we have designed a superconducting RF low-pass filter for cryogenic detector and qubit readout. The simulation shows the designed LPF has a cut-off frequency at about 30 GHz, less than 0.2 dB of insertion loss below 10 GHz and more than 30 dB attenuation in the stop-band up to at least 200 GHz. Our design is based on artificial transmission line which can be easily engineered to set the cut-off frequency. The feed-line is made of low T_c material so that above the gap frequency the feed-line becomes resistive to attenuate the transmission in the stop-band. We also use microwave absorber and aperiodic unit structures to suppress the cavity resonances and spurious pass-band. Our LPF design offers the advantages of close-to-zero insertion loss below 10 GHz, precise and sharp frequency cut-off, and linear phase response. Assembled with RF connectors, one can make a separate and compact LPF package which can be easily integrated with other microwave circuits at low temperature.

Appendix

Here, we show a 1-port simulation for 8-unit design to obtain the unit reactance C_u and L_u, which is shown in Fig. 6. For C_u simulation, the feed-line is open ended (see Fig. 6b). We can obtain the total capacitance to the ground for the 8 units in parallel

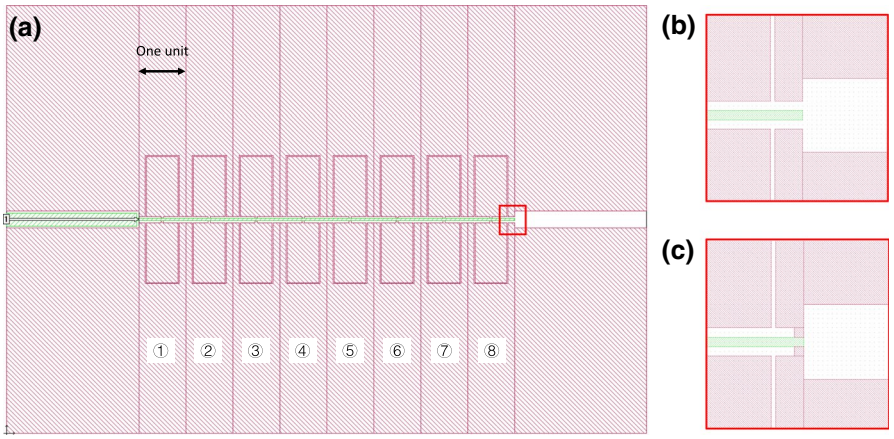

Fig. 6 (color online) **a** A single-port simulation for a 8-unit structure. **b** The feed-line is open ended for capacitance simulation. **c** The feed-line is short ended for inductance simulation

from the imaginary part of the input impedance Z_{11}: $C_{total} = -1/(2\pi f * \text{imag}(Z_{11}))$. Then, the capacitance of the single unit to the ground is given by $C_u = C_{total}/8$. For L_u simulation, the feed-line is short ended to ground by two slots (see Fig. 6c). The total inductance of the 8 units in series can be obtained from: $L_{total} = \text{imag}(Z_{11})/(2\pi f)$. Note that the inductance of the grounding part on the edge should be much smaller than the feed-line inductance in order to get accurate L_{total}. Then, the inductance of the single unit is given by $L_u = L_{total}/8$. Actually, if the feed-line is made from high kinetic inductance film with sheet inductance L_k, then the unit inductance can be estimated by $L_k * N$, where N is the number of squares for one-unit feed-line.

Acknowledgments This work was supported in part by the National Natural Science Foundation of China (Grant Nos. 61871333 and 11974290), and the Natural Science Foundation of Sichuan (Grant No. 2022NSFSC0518).

Data Availability The datasets generated during and/or analyzed during the current study are available from the corresponding author on reasonable request.

References

1. R. Dassonneville, T. Ramos, V. Milchakov, L. Planat, É. Dumur, F. Foroughi, J. Puertas, S. Leger, K. Bharadwaj, J. Delaforce, C. Naud, W. Hasch-Guichard, J.J. García-Ripoll, N. Roch, O. Buisson, Phys. Rev. X **10**, 011045 (2020). https://doi.org/10.1103/PhysRevX.10.011045
2. F. Lecocq, F. Quinlan, K. Cicak, J. Aumentado, S.A. Diddams, J.D. Teufel, Nature **591**, 575–579 (2021). https://doi.org/10.1038/s41586-021-03268-x
3. A.D. Córcoles, J.M. Chow, J.M. Gambetta, C. Rigetti, J.R. Rozen, G.A. Keefe, M.B. Rothwell, M.B. Ketchen, M. Steffen, Appl. Phys. Lett. **99**, 181906 (2011). https://doi.org/10.1063/1.3658630
4. I.M. Pop, K. Geerlings, G. Catelani, R.J. Schoelkopf, L.I. Glazman, M.H. Devoret, Nature **508**, 369 (2014). https://doi.org/10.1038/nature13017
5. G.D. Lange, J. Low Temp. Phys. **176**, 408–413 (2014). https://doi.org/10.1007/s10909-013-1046-8
6. K. Kakuyanagi, T. Meno, S. Saito, H. Nakano, K. Semba, H. Takayanagi, F. Deppe, A. Shnirman, Phys. Rev. Lett. **98**, 047004 (2007). https://doi.org/10.1103/PhysRevLett.98.047004
7. R. Barends, J. Wenner, M. Lenander, Y. Chen, R.C. Bialczak, J. Kelly, E. Lucero, P. O'Malley, M. Mariantoni, D. Sank, H. Wang, T.C. White, Y. Yin, J. Zhao, A.N. Cleland, J.M. Martinis, J.J.A. Baselmans, Appl. Phys. Lett. **99**, 080502 (2011). https://doi.org/10.1063/1.3638063
8. F.P. Millikena, J.R. Rozen, G.A. Keefe, and R. H. Koch Rev. Sci. Instrum. **78**, 024701 (2007). https://doi.org/10.1063/1.2431770
9. D.F. Santavicca, D.E. Prober, Meas. Sci. Technol. **19**, 087001 (2012). https://doi.org/10.1088/0957-0233/19/8/087001
10. A. Lukashenko, A. Ustinov, Rev. Sci. Instrum. **79**, 014701 (2008). https://doi.org/10.1063/1.2827515
11. K. Bladh, D. Gunnarsson, E. Hürfeld, S. Devi, C. Kristoffersson, B. Smålander, S. Pehrson, T. Claeson, P. Delsing, Rev. Sci. Instrum. **74**, 1323–1327 (2003). https://doi.org/10.1063/1.1540721
12. M. Hashisaka, Y. Yamauchi, K. Chida, S. Nakamura, K. Kobayashi, T. Ono, Rev. Sci. Instrum. **80**, 2519 (2009). https://doi.org/10.1063/1.3227029
13. Oliver Heaviside's Work, Nature **129**, 642–644 (1932). https://doi.org/10.1038/129643b0
14. M. Malnou, M.R. Vissers, J.D. Wheeler, J. Aumentado, J. Hubmayr, J.N. Ullom, J. Gao, PRX Quantum **2**, 010302 (2021). https://doi.org/10.1103/PRXQuantum.2.010302
15. S. Chaudhuri, D. Li, K.D. Irwin, C. Bockstiegel, J. Hubmayr, J.N. Ullom, M.R. Vissers, J. Gao, Appl. Phys. Lett. **110**, 152601 (2017). https://doi.org/10.1063/1.4980102
16. C. Bockstiegel, Y. Wang, M.R. Vissers, L.F. Wei, S. Chaudhuri, J. Hubmayr, J. Gao, Appl. Phys. Lett. **108**, 222604 (2016). https://doi.org/10.1063/1.4953209

17. J. Krupka, J. Breeze, A. Centeno, N. Alford, T. Claussen, L. Jensen, IEEE Trans. Microw. Theory. Tech. **54**, 3995 (2006). https://doi.org/10.1109/TMTT.2006.883655
18. J. Gao, M.R. Vissers, M. Sandberg, D. Li, H.M. Cho, C. Bockstiegel, B.A. Mazin, H.G. Leduc, S. Chaudhuri, D.P. Pappas, K.D. Irwin, J. Low Temp. Phys. **176**, 136–141 (2014). https://doi.org/10.1007/s10909-014-1089-5
19. https://www.sonnetsoftware.com/
20. A. Endo, A.P. Laguna, S. Hähnle, K. Karatsu, D.J. Thoen, V. Murugesan, J.J.A. Baselmans, SPIE **11453**, 436 (2020). https://doi.org/10.1117/12.2560458
21. https://www.laird.com/sites/default/files/DS-ECCOSORB-MF.pdf
22. M.R. Vissers, J. Gao, M. Sandberg, S.M. Duff, D.S. Wisbey, K.D. Irwin, D.P. Pappas, Appl. Phys. Lett. **102**, 232603 (2013). https://doi.org/10.1063/1.4804286
23. C. Chen, IEEE Trans. Compon. Packag. Manuf. Technol. **4**, 922–928 (2014)
24. S. Roshani, S. Roshani, Wireless Netw. **26**, 1493–1501 (2020). https://doi.org/10.1007/s11276-019-02214-0
25. S.H. Kazemi, M. Ghanbarpour, A. Zahedi, M. Hayati, AEU-Int. J. Electron. Commun. **136**, 153775 (2021). https://doi.org/10.1016/j.aeue.2021.153775